Diffusive spreading of time-dependent pressures in elastic microfluidic devices†

Bernhard K. Wunderlich, Ulrich A. Kleßinger and Andreas R. Bausch*

Received 29th September 2009, Accepted 16th December 2009
First published as an Advance Article on the web 4th February 2010
DOI: 10.1039/b920221h

Here we show that transient flow of Newtonian fluids in viscoelastic PDMS microfluidic channels can be described by a diffusive pressure spreading mechanism analogous to the electric telegrapher's equation. The pressure diffusion constant $D_p = 1/R_xC_x$ of a channel with length l is determined by the hydrodynamic resistance R_x and capacitance C_x per unit length of the channel. l^2/D_p sets the timescale for the transmission of pressure steps along the channel and the relaxation after a pressure step in steady state flow. For oscillatory flows, the channel acts as a low-pass filter with a cutoff frequency $\omega_{\mathrm{cutoff}} = 2\pi D_p l^{-2}$, so that pressure and flow rate pulses disperse and get smoothed while they travel along the channel. The combination of different microparticle tracking techniques allows the determination of pressure and flow profiles at any point in the channel and excellent agreement with theoretical predictions is obtained.

1 Introduction

Efficient control of spatiotemporally changing pressure and flow rates is still posing a major challenge for the broad applicability of microfluidic devices. The vast majority of microfluidic devices consist of channels imprinted into a block of the elastomeric material PDMS which is bonded to a glass substrate.[1] The cheap and easy lithographic production, optical transparency, good thermal stability, high biocompatibility of the surface and the high gas permeability, which enables oxygen supply for living cells, makes PDMS particularly suited for life-science applications. Different promising approaches based on the elastic properties of PDMS have been proposed for the construction of flow-regulatory devices,[2,3] valves[4–12] and pumps.[13,14] An emerging concept is the exploitation of the frequency response of microfluidic devices for fluid control comprising mixing, valves and droplet positions.[15,16] While membrane valves are constructed by constricting the fluid channels, pumps can be constructed on the base of membrane valves rectifying a previously generated oscillatory flow.[13,15,17] The frequency response of devices is also important for microrheological applications, where the behavior of complex fluids is studied in such devices.[18,19] A long standing interest in complex fluid flows in different geometries comes from medical applications — understanding vessel diseases needs a quantitative understanding of cardiovascular flow behavior in elastic channels.

Already in 1957, the transport of blood flow through tubes was modeled by the telegrapher's equation and experimentally tested on the length scale of macrocirculation.[20–25] In this regime blood behaves essentially like a Newtonian fluid and inertia effects are important.[26] Microfluidic technology now enables us also to explore the regime of microcirculation, where inertia is negligible but the non-Newtonian properties of blood may dominate.[26] As with standard microfluidic technology almost any complex 2D geometry is readily available and the viscoelastic properties of the PDMS walls can be tuned by varying the amount of cross-linkers, microfluidics may allow building and examination of increasingly more complex model systems of the capillary system and set the stage for an experimental link between the macro- and microcirculatory regimes.[27–33] To this end, it is necessary to have a quantitative understanding of the simple case of a Newtonian fluid even in a straight channel.

In this paper we discuss how the viscoelasticity of the channel material in microfluidic devices couples to transient flows and compare theoretical with experimental results for a straight, rectangular channel with periodically applied pressure pulses. The combination of different microparticle tracking techniques allows the determination of pressure and flow profiles at any point in the channel. Based on the diffusive spreading of the pressure propagation, the fluid flow in microfluidic devices can be described as fully analogous to the electric telegrapher's equation, where here the impedance of the device is set by the viscoelastic properties of the PDMS. For all applications a simple physical basis for the frequency response of the transport properties of microfluidic devices is provided, enabling a quantitative design approach for increasingly more complex devices.

2 Theoretical description of microfluidic channel with viscoelastic walls

The effect of a tethered channel of length l, width w and height h with viscoelastic walls on the fluid flow is governed by the channel geometry and the fluid viscosity, which is summarized in the hydrodynamic resistance per unit length (R_x), the viscoelasticity of the walls, corresponding to the complex, frequency-dependent impedance per unit length ($Z_x(\omega)$) and the fluid inertia, which sets the inductance per unit length (L_x).[34,35] The complex impedance $Z_x(\omega)/\mathrm{d}x = (g_x(\omega)\mathrm{d}x)^{-1} + (i\omega C_x(\omega)\mathrm{d}x)^{-1}$ representing the wall consists of a resistance $(g_x\mathrm{d}x)^{-1}$ connected

Lehrstuhl für Zellbiophysik E27, Technische Universität München, Garching, Germany. E-mail: abausch@ph.tum.de

† Electronic supplementary information (ESI) available: Data evaluation and calculation of theoretical curves. See DOI: 10.1039/b920221h

in series with a capacitance $C_x\mathrm{d}x$, which corresponds respectively to the viscous dissipation and the elastic storage terms of the PDMS (Fig. 1). These terms can directly be matched with the elastic (G′) and viscous (G″) part of the complex shear modulus G* of the PDMS, determined by a conventional rheometer. This calibration step can be used to compute the pressure p from the measured displacement of the wall (see ESI†). Realizing that the pressure p and the flow Q correspond to the voltage and current in an electrical equivalent circuit[20] (Fig. 1b), the flow behaviour can be described by the following differential equations, which are similar to the telegrapher's equation:

$$-\frac{\partial p}{\partial t} = \frac{1}{g_x}\cdot\frac{\partial^2 Q}{\partial x\,\partial t} + \frac{1}{C_x}\frac{\partial Q}{\partial x} \tag{1}$$

$$-\frac{\partial p}{\partial x} = R_x Q + L_x\frac{\partial Q}{\partial t}$$

In a typical experiment, a periodic step pulse in pressure with frequency ω_0 is applied to the channel entrance at $x = 0$, the channel end at $x = l$ is held at ambient pressure. The resulting periodic pressure and flow rate pulses $p(x,t) = \sum_{n=0}^{\infty} p_n(x,t)$ and $Q(x,t)=\sum_{n=0}^{\infty} Q_n(x,t)$ can be best described as the discrete sum over all frequencies, where $p_n(x,t) = \Pi_n(x)\exp(i\omega_n t)$ and $Q_n(x,t) = \Theta_n(x)\exp(i\omega_n t)$ are the Fourier components with frequencies $\omega_n = n\omega_0$ and complex amplitudes Π_n and Θ_n. With these boundary conditions the solution to eqn (1) can easily be obtained using the applied pressure pulse at $x = 0$, $p(0,t)=\sum_{n=0}^{\infty} \Pi_{0n}\exp(i\omega_n t)$:

$$p_n(x,t) = \Pi_{0n}\frac{\sinh[\lambda_n(l-x)]}{\sinh[\lambda_n l]}\exp(i\omega_n t) \tag{2}$$

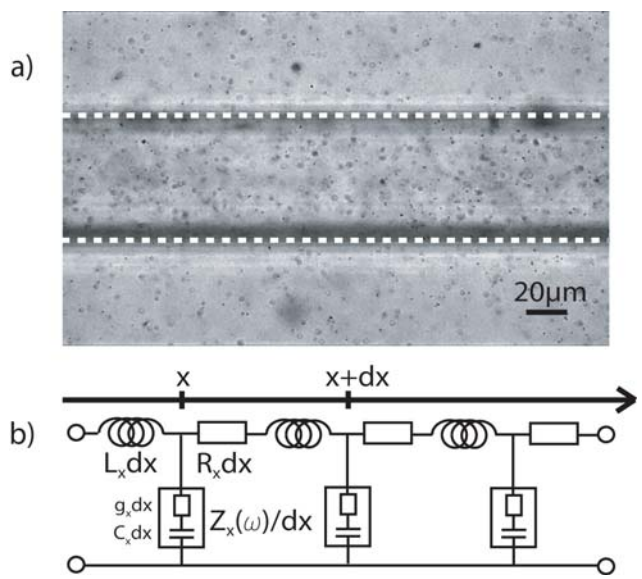

Fig. 1 a) Bright-field-videoframe of the fluid filled channel with tracer beads in the fluid and in the PDMS matrix; the dotted lines indicate the position of the channel walls, the scale bar represents 20 μm. b) Equivalent circuit with the hydrodynamic resistance $R_x\mathrm{d}x$, hydrodynamic inductance $L_x\mathrm{d}x$ and the complex impedance $Z_x(\omega)/\mathrm{d}x$ describing the viscoelastic properties of the PDMS.

$$Q_n(x,t) = \Pi_{0n}\frac{\lambda_n}{R_x + i\omega_n L_x}\frac{\cosh[\lambda_n(l-x)]}{\sinh[\lambda_n l]}\exp(i\omega_n t)$$

where $\lambda_n = \sqrt{[i\omega_n R_x C_x(1 + i\omega_n L_x/R_x)]/(1 + i\tan\delta)}$ with $\tan\delta = \omega_n C_x/g_x$.

In most microfluidic applications with typical operation frequencies ($\omega < 100$ rad s^{-1}) the Womersley parameter $\alpha = \sqrt{wh\omega/\nu}$ is small ($\alpha \leq 1$) (ν: kinematic viscosity of the fluid), so that we can neglect the inertial forces ($L_x \approx 0$). For water and blood in channels of microcirculatory diameter (100×100 μm^2 channel) $\alpha \leq 1$ holds up to frequencies of $\omega_{\alpha=1} \approx 100$ rad s^{-1} and 350 rad s^{-1}, respectively. Only in larger elastic channels like bigger blood vessels inertial effects must be taken into account, *e.g.* for blood in an aorta with 1 cm^2 cross-section: $\omega_{\alpha=1} \approx 0.035$ rad s^{-1}. Inertial terms due to transversal acceleration of the fluid (convectional terms) will be even smaller, so that the use of the 1D model is a good approximation for flow in typical microfluidic channels.

With $L_x = 0$ eqn (1) reduces for each Fourier component to

$$\frac{\partial p_n}{\partial t} = \frac{1 + i\tan\delta}{R_x C_x}\frac{\partial^2 p_n}{\partial x^2} \tag{3}$$

Except for the small viscoelastic correction term $i\tan\delta$ eqn (3) resembles the 1D-diffusion equation with the pressure diffusion coefficient $D_p = \frac{1}{R_x C_x}$. Thus eqn (3) describes the pressure propagation along the channel basically as a diffusive process like the development of a chemical concentration gradient or the heat distribution over time. The analogy to diffusion implies several characteristic features of elastic channels, which are manifested by the pressure and flow propagation inside the channels.

To test the implications, we apply periodically a pressure step pulse (0.5 Hz) into a straight microfluidic channel and observe the local pressure and flow conditions as a function of the position in the channel. To this end 1 μm beads were embedded in the PDMS as well as suspended in the fluid (Fig. 1a). Their trajectories were determined by particle tracking routines at different positions along the channel ($x = 0$, 7.5, 12.5, 17.5 mm). These were then used to evaluate the local pressures and flow rates in the channel (see Fig. 2). From the obtained results a Fourier transformation is computed in order to resolve the frequency dependencies of pressure p and flow rate Q depicted in Fig. 3 and 4 (see Materials and methods and ESI†).

3 Results and discussion

The timescale for pressure and flow pulse propagation is given by the pressure diffusion constant D_p

While in bulk fluids any excitation will propagate with the speed of sound v_c, the typical wavelength of pressure waves can not be accommodated by the channel dimensions of microfluidic devices and thus the propagation of *e.g.* a pressure pulse in a microfluidic device will be limited by its mechanical and geometrical properties. Considering eqn (3), the traveling time for crossing the whole channel length l in the low frequency limit ($\omega \ll \omega_{\mathrm{cutoff}} = 2\pi D_p l^{-2}$) is given by $\tau(0\rightarrow l) = \frac{l^2}{6\cdot D_p}$. For the

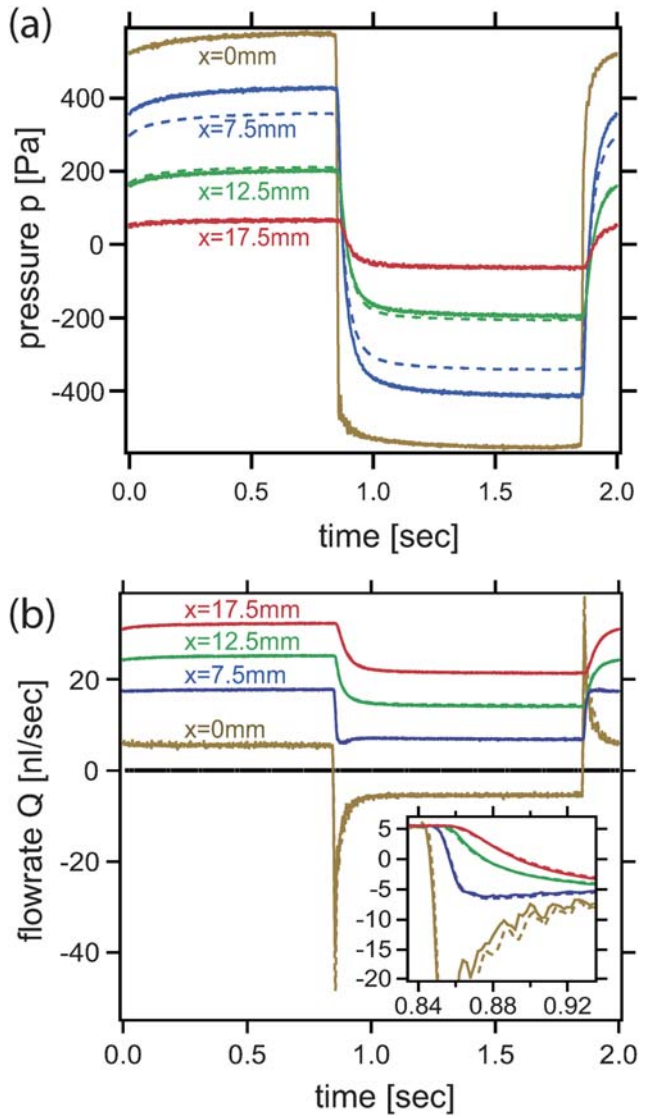

Fig. 2 Pressure p and flow rate Q pulses at $x = 0$, 7.5, 12.5, 17.5 mm in the time domain. (a) pressure pulses, (b) flow rates (solid: measured, dashed: theory); flow rates at $x = 7.5$, 12.5, 17.5 mm were offset in Q for better visibility. Inset: close up of the measured flow rates without offset showing the lag-time between flow rate pulses.

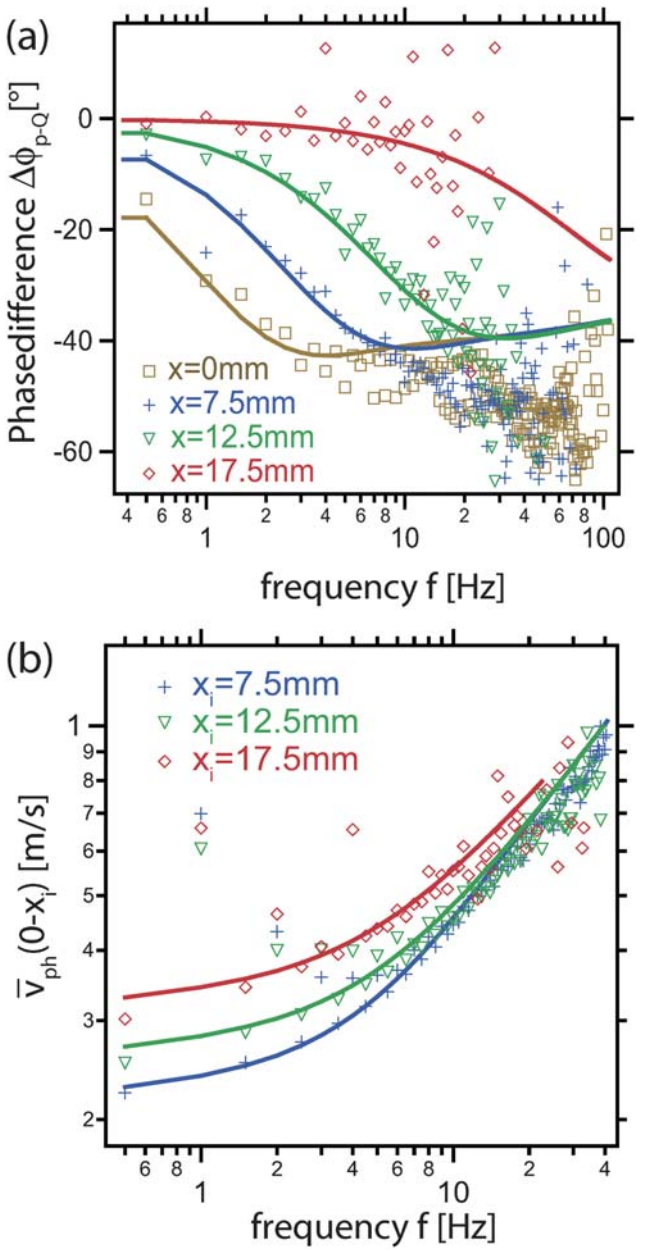

Fig. 3 Dispersion of propagating pulses (symbols: experimental values, solid lines: theoretical values): (a) phase difference $\Delta\phi_{p-Q}$ between p_n and Q_n at $x = 0$, 7.5, 12.5, 17.5 mm. $\Delta\phi_{p-Q}$ grows with frequency and decreases towards the channel exit. (b) averaged phase velocity of pressure components p_n travelling from $x = 0$ to $x_i = 7.5$, 12.5, 17.5 mm.

20 mm long channel used here the characteristic time $\tau_{RC} = R_x C_x l^2$ is approximately 0.35 s. This gives an average low frequency phase velocity for pressure propagation across the channel $\bar{v}_{ph} \approx 0.34\ \mathrm{ms}^{-1}$ which is 3 orders of magnitude below the speed of sound v_c of the fluid. The increasing lag time in the onset of the flow rate pulses (see close up in Fig. 2b) shows clearly the predicted time delay of the concomitant flow rate propagation at the different positions along the channel.

Pressure and flow pulses are subject to dispersion

The description by a diffusion equation implies that the velocity becomes frequency dependent and higher frequency components propagate faster. Consequently, the phase velocity (see ESI†) shows dispersion which is frequency and spatially dependent. This results in a phase difference between the pressure p_n and flow Q_n along the channel, which is frequency dependent and decreases along the channel length reaching zero at the exit. The phase shift can maximally be $\Delta\phi_{p-Q} = \pi/4$, which results directly from the solution for $\lambda_n = \sqrt{i\omega_n R_x C_x}$ for the case of an ideal elastic boundary ($\tan\delta = 0$). Mechanistically, one can imagine that the elastic expansion of the channel creates a local extra volume $V_{ex} \propto p_n$ in phase with the pressure. In turn the flow into this extra volume $Q_{ex} \propto \partial V_{ex}/\partial t$ needs to be $\pi/2$ ahead of the pressure. This phase shift of the flow into the extra volume results in a phase shift of the total flow $\Delta\phi_{p-Q}$ to the applied pressure. As the pressure drops along the channel, this extra volume

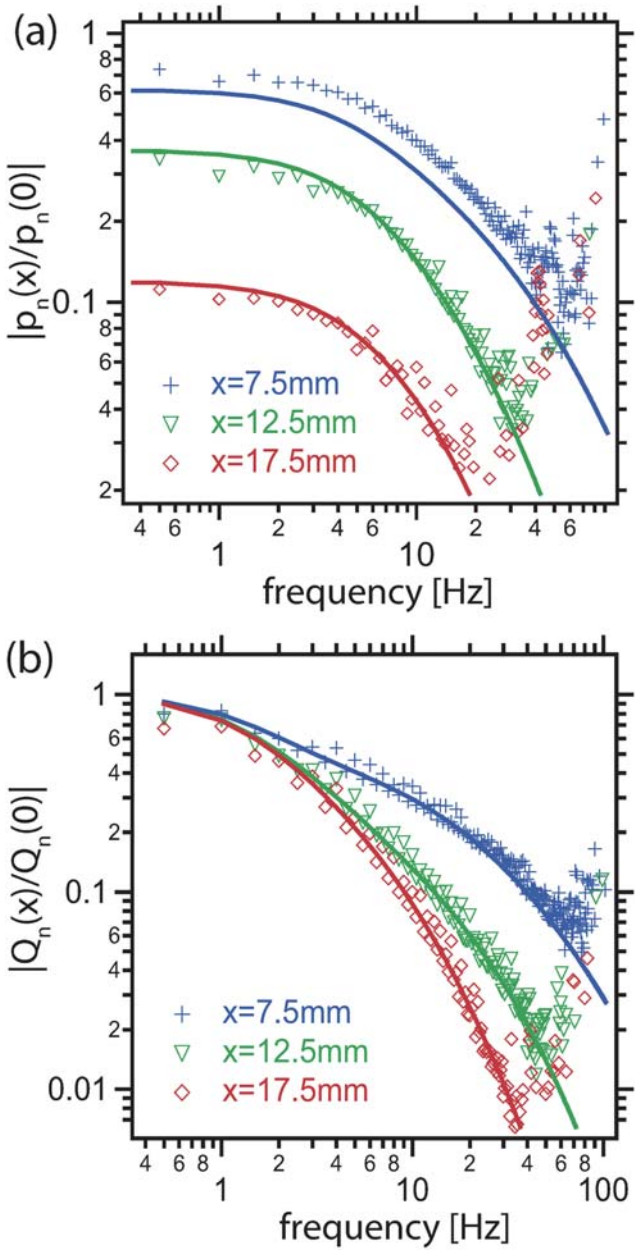

Fig. 4 Frequency dependence of (a) the pressure and (b) the flow rate transmission along the channel: Fourier components $|p_n(x)|$, $|Q_n(x)|$ normalized to their values $|p_n(0)|$, $|Q_n(0)|$ at the channel entrance. Symbols: measured values, solid lines: theoretical curves calculated from eqn (2).

decreases. Consequently, the contribution of the flow into the extra volume with respect to the transported volume decreases and thus $\Delta\phi_{p-Q}$ approaches zero. With increasing frequency the phase shift $\Delta\phi_{p-Q}$ increases, due to the simple fact, that the total volume transported per oscillation period is smaller at high frequencies, yet the extra volume is independent with frequency (neglecting damping effects).

For $\omega \ll \omega_{\text{cutoff}}$ the phase velocity $v_{ph}(x) \approx 3D_p/(l-x)$ is independent of ω and p_n and Q_n are in phase everywhere in the channel. For $\omega \gg \omega_{\text{cutoff}}$ the phase velocity $v_{ph}(\omega) \approx \sqrt{2\omega D_p/(\cos\delta(1-\sin\delta))}$ becomes independent of x, yet it grows with $\omega^{1/2}$: now the flow rate Q_n is ahead of the pressure p_n (up to $\Delta\phi_{p-Q} = \pi/4 - \delta/2$) and only at the exit (at $x \approx l$) p_n and Q_n are in phase. Fig. 3a shows the theoretically and experimentally determined values for the phase difference $\Delta\phi_{p-Q}$ as a function of the frequency $f = \frac{\omega}{2\pi}$, which are in excellent agreement. To enable a direct comparison of the computed $v_{ph}(x)$ with experimental results we need to define an averaged phase velocity $\bar{v}_{ph}(\omega)$. To this end the phase of a pressure pulse is determined at two points ($x = 0$ and $x = x_i$) for each frequency component and the resulting phase difference $\Delta\phi^{n,p}_{0-x_i}$ is used to obtain $\bar{v}_{ph}(\omega_n) = x_i\omega_n/\Delta\phi^{n,p}_{0-x_i}$. Fig. 3b shows that the frequency dependence of the measured propagation speeds is in excellent agreement with the theoretical calculations. As an important consequence from the dispersion relation the occurrence of peaks in the flow rate is expected, once a step pulse is applied. Indeed, Fig. 2 shows the dispersion of pressure p and flow rate Q pulses in the time-domain. For steep pressure pulses, the phase shift of the high-frequency components generates peaks in the flow rate at the channel entrance which can significantly exceed the steady state value ($Q_{\text{peak}} \gg p_{\text{peak}}/R_x l$). This is an important consequence of the susceptibility of microfluidic devices, which needs to be accounted for if critical shear rates need to be considered.

The microfluidic channel is a low pass to pressure and flow pulses

In addition to the dispersion, high-frequency components are damped by the diffusive-like process, resulting in an effective low-pass filter property of microfluidic devices. If the frequency of a pressure signal is faster than the time it takes to propagate to a certain position in the device, it will be smeared out beyond the diffusion length of the device. Consequently, high frequency components p_n, Q_n of pressure and flow rate pulses get damped.

The characteristic time τ_{RC} sets a cutoff frequency $\omega_{\text{cutoff}} = 2\pi/\tau_{RC}$ for the transmission of flow and pressure pulses for the whole device length. For $\omega_n \ll \omega_{\text{cutoff}}$ eqn (3) becomes $\frac{\partial^2 p}{\partial x^2} \approx 0$ and the pressure drops linearly across the channel. For $\omega_n \gg \omega_{\text{cutoff}}$ the damping becomes exponential and can be calculated for the pressure $|p_n(x)| \approx |\Pi_{0n} e^{-2\lambda_n x}|$ and for the flow rate $|Q_n(x)| \approx |\frac{\Pi_{0n}}{R_x}\lambda_n e^{-2\lambda_n x}|$. Fig. 4 shows the low-pass characteristics of the channel for normalized pressure and flow rate pulses $|p_n(x)/p_n(0)|$, $|Q_n(x)/Q_n(0)|$. Experimental values (symbols) and theoretical curves (solid lines) are again in good agreement.

4 Conclusion

The flow of Newtonian liquids in viscoelastic microfluidic channels can be described with a pressure diffusion equation. The PDMS channel acts as a low-pass filter: Fourier components with frequencies higher than ω_{cutoff} are dispersed and damped. Thus the channel effectively smooths incoming pressure and flow pulses. To generate a uniform flow along the channel, PDMS devices should only be operated with $\omega < \omega_{\text{cutoff}}$ which gives an upper limit *e.g.* for the operating frequency of switches and microchannel-rheometers. Sharp pressure pulses result in peaks of high flow rates in the channel entrance region and must be avoided in all applications that are sensitive to high wall shear

stresses. Although these high flow rate peaks are limited to the channel entrance region, sharp changing pressure pulses that temporarily give rise to very high wall shear stresses could *e.g.* be used to enhance the effectivity of cleaning processes in elastic channels. The introduced method of pressure sensing by wall-motion-tracking provides a tool for further detailed investigation of transient flows in viscoelastic channels. The presented experimental approach as well as the modeling may provide a useful basis for studies of non-Newtonian-liquids in any 2-D geometry achieved with the standard PDMS soft lithography procedure. It should be well suited for simulating flows in small to intermediate blood vessels with different geometries – although in these cases inertia effects need to be accounted for.

5 Materials and methods

The microfluidic channel with length $l = 20$ mm, width $w = 60$ μm and height $h = 80$ μm was fabricated following the standard protocol.[1] PDMS and cross-linker (SYLGARD 184 Silicone Elastomer Kit) were mixed in a ratio of 20 : 1 and cured for 2 h at 70 °C to yield soft channels with well defined viscoelasticities. 1 μm melamine resin beads (microparticles GmbH, Berlin) were used to track the motion of the channel walls. They were suspended in the crosslinker solution prior to mixing. The channel was filled with a suspension of the same 1 μm beads in approximately 60% (w/v) glycerol water solution. A speaker was coupled to the membrane of a fluid reservoir which was connected with the microfluidic channels *via* $d = 0.5$ mm metal and polymeric tubing. Rectangular voltage signals of ±0.4 V and 0.5 Hz were applied to the speaker to generate periodic pressure pulses at the channel entrance ($x = 0$). The other end of the channel ($x = 20$ mm) was connected to a small reservoir exposed to ambient pressure. A videoframe of the measurement shows the tracer beads in the fluid and in the PDMS matrix recorded through a bright field microscope (Axiovert 200, 63× long distance objective) with a high-speed camera (Phantom V5.1, Vision Research) at 500 fps in the midplane of the channel at $z = 0.5h$ (Fig. 1a).

Acknowledgements

This work was supported by the Nanosystems Initiative Munich (NIM) and the EU Sixth Framework Programme under Contract 033339.

References

1 J. McDonald and G. Whitesides, *Acc. Chem. Res.*, 2002, **35**, 491–499.
2 Y. Kim, B. Kuczenski, P. LeDuc and W. Messner, *Lab Chip*, 2009, **9**, 2603–2609.
3 B. Yang and Q. Lin, *J. Microelectromech. Syst.*, 2007, **16**, 411–419.
4 M. A. Unger, H.-P. Chou, T. Thorsen, A. Scherer and S. R. Quake, *Science*, 2000, **288**, 113–116.
5 A. R. Abate and D. A. Weitz, *Appl. Phys. Lett.*, 2008, **92**, 243509.
6 J. Baek, J. Park, J. Ju, T. Lee and S. Lee, *J. Micromech. Microeng.*, 2005, **15**, 1015–1020.
7 J. Kim, J. Baek, K. Lee, Y. Park, K. Sun, T. Lee and S. Lee, *Lab Chip*, 2006, **6**, 1091–1094.
8 W. Gu, X. Zhu, N. Futai, B. Cho and S. Takayama, *Proc. Natl. Acad. Sci. U. S. A.*, 2004, **101**, 15861–15866.
9 J. Loverich, I. Kanno and H. Kotera, *Microfluid. Nanofluid.*, 2007, **3**, 427–435.
10 E. Hasselbrink, T. Shepodd and J. Rehm, *Anal. Chem.*, 2002, **74**, 4913–4918.
11 J. Go and S. Shoji, *Sens. Actuators, A*, 2004, **114**, 438–444.
12 S. Lee, W. Jeonga and D. Beebe, *Lab Chip*, 2003, **3**, 164–167.
13 N. Jeon, D. Chiu, C. Wargo, H. Wu, I. Choi, J. Anderson and G. Whitesides, *Biomed. Microdevices*, 2002, **4**, 117–121.
14 N. Graf and M. Bowser, *Lab Chip*, 2008, **8**, 1664–1670.
15 D. C. Leslie, C. J. Easley, E. Seker, J. M. Karlinsey, M. Utz, M. R. Begley and J. P. Landers, *Nat. Phys.*, 2009, **5**, 231–235.
16 S. Langelier, D. Chang, R. Zeitoun and M. Burns, *Proc. Natl. Acad. Sci. U. S. A.*, 2009, **106**, 12617–12622.
17 J. Loverich, I. Kanno and H. Kotera, *Lab Chip*, 2006, **6**, 1147–1154.
18 Y.-L. Chen, M. D. Graham, J. J. de Pablo, K. Jo and D. C. Schwartz, *Macromolecules*, 2005, **38**, 6680–6687.
19 K. Jo, Y.-L. Chen, J. J. de Pablo and D. C. Schwartz, *Lab Chip*, 2009, **9**, 2348–2355.
20 M. Taylor, *Phys. Med. Biol.*, 1957, **1**, 258–269.
21 M. Taylor, *Phys. Med. Biol.*, 1957, **1**, 321–329.
22 J. Womersley, *Phys. Med. Biol.*, 1957, **2**, 178–187.
23 J. T. M. Klanchar and D. Wang, *Circ. Res.*, 1990, **66**, 1624–1635.
24 A. Khir, A. O'Brien, J. Gibbs and K. Parker, *J. Biomech.*, 2001, **34**, 1145–1155.
25 A. Khir and K. Parker, *J. Biomech.*, 2002, **35**, 775–783.
26 C. Caro, K. Parker and D. Doorly, *Perfusion*, 1995, **10**, 131–134.
27 R. Amenzadeh, *Dokl. Phys.*, 2008, **53**, 39–42.
28 A. R. Ramachandra, *Acta Mechanica*, 1983, **46**, 155–165.
29 D. Wang and J. Tarbell, *J. Biomech. Eng.*, 1995, **117**, 127–135.
30 X. Qi, D. Scott and D. Wilson, *Chem. Eng. Sci.*, 2008, **63**, 2682–2689.
31 L. Formaggia, D. Lamponi and A. Quarteroni, *J. Eng. Math.*, 2003, **47**, 251–276.
32 S. Sherwin, V. Franke, J. Peiro and K. Parker, *J. Eng. Math.*, 2003, **47**, 217–250.
33 J. Alastruey, K. Parker, J. Peiro and S. Sherwin, *Commun. Comput. Phys.*, 2008, **4**, 317–336.
34 H. Bruus, *Theoretical Microfluidics*, Oxford University Press, 2007.
35 W. Nichols, *McDonald's Blood Flow in Arteries*, Oxford University Press, 2005.